# GNSS-Over-Fiber Sensing System for High Precision 3D Nodal Displacement and Vibration Detection

Xin Jiang, Chaosheng Huang, Xiangchuan Wang, Xi Liu, Lihan Wang, Feng Wang, *Senior Member, IEEE*, Jianbin Fu, Zhongyang Xu, *Member, IEEE*, and Shilong Pan, *Fellow, IEEE*

***Abstract*— Aiming at realizing comprehensive structural health monitoring, a GNSS (Global Navigation Satellite System) over fiber sensing approach is presented and experimentally demonstrated to achieve 3D nodal displacement and vibration detection simultaneously. GNSS signals from multi-antennas are transferred to a receiver based on an optical fiber link, also used as distributed sensing fiber. Broadband linear frequency-modulated (LFM) probe light with high linearity is generated based on electro-optic modulation to probe distributed vibrations and monitor the transmission time delay along the whole fiber with high precision. The spectral components generated by vibrations are detected using the cross-correlation method to achieve distributed vibration sensing. In addition, with the assistance of high-precision hardware-delay measurement, the variation of transmission time delay can be obtained, improving the precision of 3D displacement measurement in the GNSS-over-fiber architecture. In the proof-of-concept experiment, a 3D baseline can be obtained with the precision of 2.8, 3.6, and 2.0 mm, while vibrations with frequencies of 40 kHz, 80 kHz, and 100 kHz along 250 m fiber are successfully detected with a spatial resolution of 1 m.**

***Index Terms*— GNSS-over-fiber, displacement measurement, distributed fiber sensing, vibration sensing, optical time delay measurement.**

## I. Introduction

DISPLACEMENT and vibration are key parameters for sensing systems, which have been applied to monitor the structure loading and damage-provoking conditions for structural health monitoring and risk prediction purposes. For example, it is usually important to monitor the bridge deck and pier simultaneously in practice. As the bridge deck is long-range, distributed monitoring is suitable, whereas 3D nodal and high-precision displacement is more appropriate for bridge pier monitoring. In addition, aiming at aircraft health status evaluation, flight condition monitoring requires 3D attitude measurement, while the structure health monitoring needs distributed sensing to achieve an integrated system.

In the past several decades, several displacement measurement technologies, including indirect and direct measurement methods, have been proposed. The indirect measurement methods are mainly based on the relationship between strain and displacement. Typically, strain sensing can be realized by fiber Bragg grating (FBG), which converts the strain to the wavelength shift [1], [2]. Thus 2D displacement can be obtained. Furthermore, 3D shape sensing can be realized by utilizing a multi-core fiber engraved with FBGs [3]. The key difficulty of the indirect method is establishing an accurate mapping model between strain and displacement. In addition, the measurement results are usually sensitive to temperature variation and induce cross-sensitivity. The direct measurement methods mainly include vision and image processing technique [4], radar technique [5], inertial sensing technique [6], GNSS positioning technique [7]. Among these direct methods, the GNSS positioning technique is one of the most attractive methods to measure the 3D displacement for the advantages of no intervisibility required and no error accumulation [8]. Recently, GNSS-over-fiber systems [9], [10] have been proposed to extend the measurement range and achieve high precision [11]. However, as the delay variance of the fiber link would greatly deteriorate the displacement measurement precision, the fiber is usually protected from a disturbance in the traditional GNSS-over-fiber system. Thus only key position monitoring can be achieved in the traditional GNSS-over-fiber system.

In addition to the nodal displacement measurement, vibration is another important parameter for structural health monitoring applications. Distributed optical fiber sensing (DOFS) technologies have been widely studied to measure the vibration for advantages of long-range sensing, small-size, lightweight, and immune to electromagnetic interferences, which has a great attraction to large-scale structure health monitoring. Among the DOFS technologies, optical frequency domain reflectometry (OFDR) can usually achieve high spatial resolution. However, the nonlinearity and phase noise of the probe LFM signal induced by a swept-frequency laser

Manuscript received 25 September 2022; revised 22 December 2022; accepted 22 February 2023. Date of publication 2 March 2023; date of current version 13 March 2023. This work was supported in part by the National Natural Science Foundation of China under Grant 62075095 and Grant 62171219, in part by the Young Elite Scientists Sponsorship Program by the China Association for Science and Technology (CAST) under Grant 2018QNRC001, and in part by the Key Research and Development Program of Jiangsu Province under Grant BE2020030. *(Corresponding authors: Xiangchuan Wang; Shilong Pan.)*

Xin Jiang is with the Key Laboratory of Radar Imaging and Microwave Photonics (Nanjing University of Aeronautics and Astronautics), Ministry of Education, Nanjing University of Aeronautics and Astronautics, Nanjing 210016, China, and also with the Leihua Electronic Technology Research Institute, Aviation Industry Corporation of China Ltd., Wuxi 214063, China.

Chaosheng Huang, Xiangchuan Wang, Xi Liu, Lihan Wang, Zhongyang Xu, and Shilong Pan are with the Key Laboratory of Radar Imaging and Microwave Photonics (Nanjing University of Aeronautics and Astronautics), Ministry of Education, Nanjing University of Aeronautics and Astronautics, Nanjing 210016, China (e-mail: wangxch@nuaa.edu.cn; pans@nuaa.edu.cn).

Feng Wang is with the Institute of Optical Communication Engineering, Nanjing University, Nanjing 210093, China.

Jianbin Fu is with Suzhou Liuyaosi Information Technologies Company Ltd., Suzhou 215558, China.

Color versions of one or more figures in this letter are available at https://doi.org/10.1109/LPT.2023.3251369.

Digital Object Identifier 10.1109/LPT.2023.3251369

1041-1135 © 2023 IEEE. Personal use is permitted, but republication/redistribution requires IEEE permission.
See https://www.ieee.org/publications/rights/index.html for more information.

Authorized licensed use limited to: NANJING UNIVERSITY OF AERONAUTICS AND ASTRONAUTICS. Downloaded on October 09,2024 at 02:38:19 UTC from IEEE Xplore. Restrictions apply.

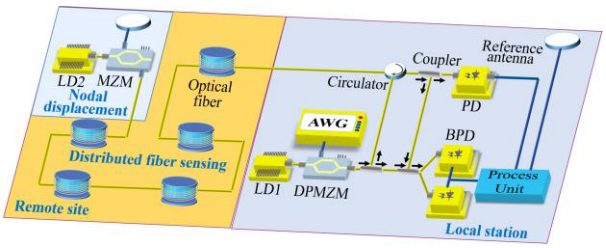


Fig. 1. Schematic diagram of the comprehensive structural health monitoring configuration (Optical paths and electrical paths are distinguished by yellow and blue). LD: laser diode; AWG: arbitrary waveform generator; PD: photodetector; MZM: Mach-Zehnder modulator; BPD: balanced photodetector; DPMZM: dual-parallel MZM.

will widen the interference signal, deteriorating the spatial resolution. Therefore, research efforts have mainly focused on the nonlinearity compensation methods to improve the performance of an OFDR-based sensing system, leading to a complex and time-consuming system. In addition, the above displacement and distributed vibration sensing systems can only be implemented separately, limiting their application in structural health monitoring.

In this letter, an integrated sensing system is proposed to achieve 3D nodal displacement and vibration detection simultaneously by reusing the same transmission fiber, signal generation, and processing part. A high-quality LFM optical signal is generated by an external modulation method to incorporate GNSS-based displacement sensing and OFDR-based vibration sensing. The proposed system has the potential for no nonlinearity compensation with an ultra-narrow linewidth laser. After spectrum analysis of the interference of LFM optical signals, the transmission delay between the antenna and receiver in a GNSS-over-fiber system can be obtained, achieving high-precision 3D nodal displacement measurement. In addition, the new frequency component introduced by vibration can be extracted by cross-correlation, realizing the distributed vibration sensing simultaneously.

## II. Principle

In the proposed integrated monitoring system, the optical fiber is pulled far from the local station to the monitored structure. The GNSS antennas are inserted into the nodes that need to focus on monitoring displacement. Meanwhile, optical fiber is utilized for distributed vibration sensing. The schematic diagram of the monitoring system is shown in Fig. 1.

At the remote site, the antenna is utilized to receive the GNSS signals. Then an optical signal generated by a laser diode (LD2) is intensity-modulated through a Mach-Zehnder modulator (MZM). The modulated optical signal is sent into a photodetector (PD) to recover the GNSS signals. In the local station, an LFM optical signal is generated based on the carrier-suppressed single-sideband (CS-SSB) modulation [12]. The LFM optical signal is then sent into the optical transmission fiber by a circulator. The interference of the reflected and backscattered optical signals generates the beating signal by a balanced photodetector. To distinguish the GNSS signal and LFM signal, two separate LDs are utilized, as shown in Fig. 1. The carrier frequencies of GNSS signals are from 1-2 GHz while the center frequency of the intermediate frequency LFM signal is 10.5 GHz.

In a GNSS-over-fiber based 3D baseline measurement system, there are three main measurement errors, which are satellite-related, propagation-related, and receiver-related. Given the same satellite, the single difference(SD) operation is obtained by making a difference in the carrier phases between two receive antennas. After the SD operation, the first two types of errors can be eliminated or greatly mitigated to less than a few millimeters. However, the receiver-related error which mainly consisted of the transmission time delay between the local receiver and the remote antenna still exists. Thus the carrier phase single difference(CPSD) model with a common-clock receiver can be presented as [10]

$$\lambda\Delta\phi_{ij}^{k} = \mathbf{s}^{k}\mathbf{b}^{T} + \Delta LB_{ij} + \lambda\Delta N_{ij}^{k} + \Delta e_{ij}^{k} \tag{1}$$

Here, $\lambda$ denotes the wavelength of the GNSS carrier, $\phi$ represents the GNSS carrier phase, $\boldsymbol{s}^{k}$ represents the normalized line of the sight vector, $N$ is the inter ambiguity of the carrier phase. The parameters mentioned above can be calculated by the GNSS processing algorithm. $\boldsymbol{b} = [\,b_{\mathrm{x}}\ b_{\mathrm{y}}\ b_{\mathrm{z}}\,]$ is the 3D baseline to be solved. *LB* represents the transmission time delay between the local receiver and the remote antenna. Besides, $\Delta$ is the SD operation, $e$ represents the measurement noise, $k$ is the satellite, $i$ and $j$ are antennas, $T$ denotes the transpose symbol. In the CPSD model, the *LB* variation should be precisely measured to obtain the 3D baseline precisely. In this work, the time delay measurement can be utilized to obtain the LB parameter.

Next, the principles of time delay measurement and vibration sensing based on OFDR are described. The optical field of the lightwave $E_r$ and the interference signal can be expressed by

$$E_r(t) = E_0 \exp\left\{j\left[2\pi f_0 t + \pi\gamma t^2 + \phi(t)\right]\right\} \tag{2}$$

$$I_s(t) = 2\sqrt{R(\tau_i)}E_0^2 \cos\left[2\pi\gamma\tau_i t + \varphi(\tau_i) + \phi(t) - \phi(t-\tau_i)\right] \tag{3}$$

Here

$$\varphi(\tau_i) = 2\pi f_0\tau_i - \pi\gamma\tau_i^2 \tag{4}$$

$E_0$ and $f_0$ are the amplitude and the initial frequency of the LFM optical signal, $\gamma$ is the tuning rate, $\sqrt{R}$ is the reflectivity of fiber at the scattering point $i$, $\tau_i$ is the transfer time delay at the scattering point $i$.

The backscattering optical signal is phase-modulated when the fiber is disturbed [13]. Under the small-signal approximation condition, the beating signal can be written as

$$\begin{aligned} I_s(t) = {} & 2\sqrt{R(\tau_i)}E_0^2\{J_0(\delta)\cos\left[2\pi\gamma\tau_i t + \varphi(\tau_i) + \phi(t) \right. \\ & \left. - \phi(t-\tau_i)\right] \\ & + J_1(\delta)\cos\left[2\pi\left(\gamma\tau_i - f_{\mathrm{Vib}}\right)t + \varphi(\tau_i) + \phi(t)\right. \\ & \left. - \phi(t-\tau_i)\right] \\ & - J_1(\delta)\cos\left[2\pi\left(\gamma\tau_i + f_{\mathrm{Vib}}\right)t + \varphi(\tau_i) + \phi(t)\right. \\ & \left. - \phi(t-\tau_i)\right]\} \end{aligned} \tag{5}$$

Here, $\delta$ is the amplitude of the vibration, $f_{Vib}$ is the frequency of the vibration, $J_0$ and $J_1$ are zeroth-order and first-order Bessel functions of the first kind, respectively.

From the formula (5), it can be concluded that the frequency difference between the new induced frequency components

Authorized licensed use limited to: NANJING UNIVERSITY OF AERONAUTICS AND ASTRONAUTICS. Downloaded on October 09,2024 at 02:38:19 UTC from IEEE Xplore. Restrictions apply.

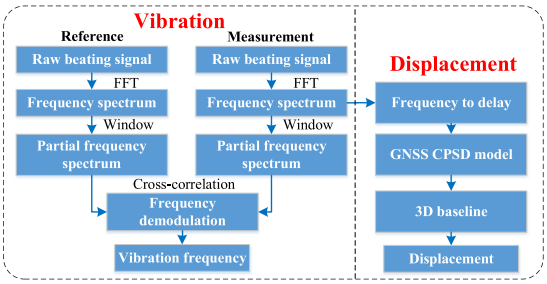


Fig. 2. The flow chart of the vibration sensing and displacement measurement.

and the original frequency component corresponds to the induced vibration frequency. Thus, the vibration frequency can be calculated according to the frequency demodulation. The LB parameter can be obtained according to the linear relationship between the original frequency and the time delay. The frequency resolution and the minimum detectable frequency depend on the period of the LFM optical signal $T$, while the max detectable frequency depends on the number $n$ of the cross-correlation points in the sliding window, which can be written as:

$$f_{\text{Vib\_min}} = 1/T, \quad f_{\text{Vib\_max}} = n \times f_{\text{Vib\_min}} \tag{6}$$

Thus the frequency resolution is 10 kHz when $T = 100$ us. The maximum measurable frequency is 500 kHz when $n = 50$.

The flow chart of the cross-correlation-based vibration sensing and GNSS-based displacement measurement is shown in Fig. 2. The detailed process is described as follows: First, the Fast Fourier Transformation (FFT) is applied to obtain the frequency spectrum information from the beating signal. Then the partial frequency spectrum of different sections along the fiber is abstracted. For displacement measurement, the frequency is converted to the time delay and helps to solve the GNSS-based 3D baseline. By fixing the reference antenna, the displacement is equivalent to the baseline variation between the remote measurement antenna and the local reference antenna. For distributed sensing, through sliding the window, a partial frequency spectrum is chosen, then the new frequency component is obtained through the cross-correlation method between the reference and the measurement data. The length of the window section is identified according to the spatial resolution and maximum measurement range. Finally, the vibration frequency can be derived from the frequency difference between the new induced frequency components and the original frequency component.

## III. Experiments

In the investigation of the vibration sensing function, the intermediate frequency LFM signal is generated by the arbitrary waveform generator (AWG) with a bandwidth of 5 GHz and a period of 100 us, which means the frequency chirp factor is $5 \times 10^4$ GHz/s. To reduce the influence of the laser noise, a narrow linewidth laser with a linewidth of less than 100 Hz is utilized. The wavelengths of the two lasers are about 1550 nm. The bandwidths of the PD and the BPD are 10 GHz and 150 MHz, respectively. The detection bandwidth requirements of the GNSS signals and the LFM optical signal are about 2 GHz and 125 MHz. The latter depends on the frequency chirp factor and the length of the

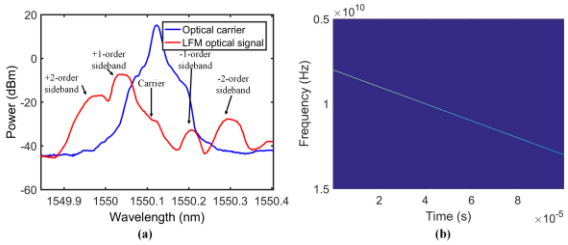


Fig. 3. (a) Spectra of the optical carrier and the LFM optical signal. (b) The instantaneous frequency of the LFM signal.

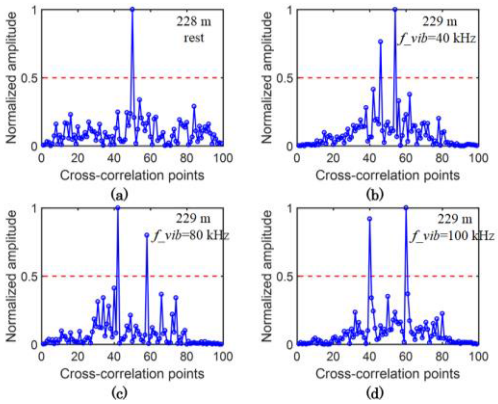


Fig. 4. The cross-correlation results between the reference data and the vibrated data.

optical transmission fiber used in our experiment, which is about 250 m. The spectra of the optical carrier and the LFM optical signal are measured by an optical spectrum analyzer (YOKOGAWA) with a resolution of about 0.02 nm, shown in Fig. 3(a). The +1-order sideband is utilized as the probe signal whose center frequency has an offset with respect to the carrier, which is equal to the center frequency of the intermediate frequency LFM signal. Compare with the +1-order sideband, the carrier-suppression ratio is about 20 dB. Meanwhile, the +2-order sideband suppression radio is about 10 dB. Then short-time Fourier transform is utilized to obtain the time-frequency graph, shown in Fig. 3(b). Furthermore, the linear goodness of fit can be calculated as about $1\text{-}10^{-6}$ with the R-squared estimator. A piezoelectric transducer (PZT) fiber stretcher with a 3 m wounded fiber is utilized as the vibration source. To sample the backscattered optical signals, a sliding window with a width of 1 m is utilized. Thus no compensation of the nonlinear frequency shift is applied because the used relatively long spatial resolution does not need it.

The cross-correlation results are shown in Fig. 4. As can be seen, when the backscattered signal is obtained in the rest position of about 228 m, a peak can be seen in Fig. 4(a). If the backscattered signal is sampled from the vibration position of about 229 m, the cross-correlation result shows other peaks in Fig. 4(b). Therefore, the spatial resolution of the distributed vibration sensor is 1 m, which is the same as the preset sliding window. To identify the vibration frequency, different vibration frequencies are utilized to simulate vibration events. The single-frequency signal with a frequency of 40 kHz, 80 kHz, and 100 kHz is adopted in the test. The experimental results are shown in Fig. 4(b), (c), and (d), in which the vibration frequencies can be calculated from the difference between the peak and the center. It can be observed that

Authorized licensed use limited to: NANJING UNIVERSITY OF AERONAUTICS AND ASTRONAUTICS. Downloaded on October 09,2024 at 02:38:19 UTC from IEEE Xplore. Restrictions apply.

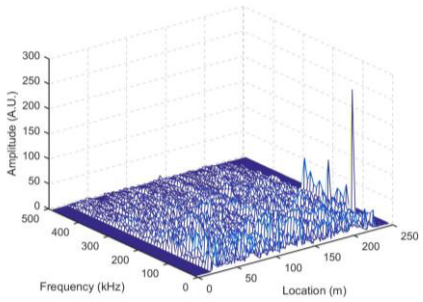


Fig. 5. The retrieved vibration frequency spectra.

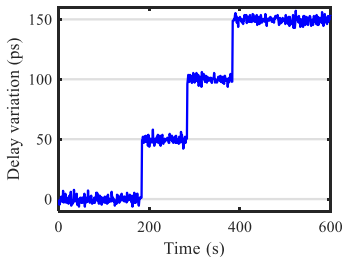


Fig. 6. The time delay variation measurement result.

the offsets are 4, 8, and 10 separately, which represent the vibration frequencies as 40 kHz, 80 kHz, and 100 kHz.

When the frequency of the driving signal is set as 80 kHz, the frequencies detected along the optical fiber are shown in Fig. 5. It can be seen that just 80 kHz vibration is detected at about 229 m, verifying the capability of distributed sensing.

With the assistance of the above system, the frequency measurement is utilized to obtain the time delay of the end of the sensing fiber with a precision of several picoseconds. In a practical case, the Fast Fourier Transformation (FFT) is applied to obtain the frequency spectrum information. Then the frequency is converted to the time delay. From equation (3), the time delay can be calculated as $\tau_i = f_s/\gamma$. Here $f_s$ is the peak frequency of the beating signal, which represents the node. After the time delay is estimated, it will be substituted into the CPSD model as the LB parameter to solve the 3D baseline. To investigate the displacement measurement function, a high-precision motorized variable optical delay line (M-VODL) is utilized as a reference for the time delay. Then the M-VODL is moved by 50 ps three times. The measured time delay variation result is presented in Fig. 6.

In terms of precision, the standard deviations of the time delay variation result are 3.03 ps, 2.67 ps, 2.57 ps, and 2.43 ps. In terms of accuracy, the means of the time delay variation are 0 ps, 49.97 ps, 100.70 ps, and 150.41 ps. The CPSD model requires a time delay measurement precision higher than 3.33 ps, which represents 1 mm in the vacuum, so the experimental results show that the proposed system is competent.

3D displacement measurement results are given in Fig. 7, showing the 3D baseline obtained by the CPSD model without and with the time delay variation compensation. If the time delay variation is not compensated, the measurement result shows significant drift with the same trend as the transmission time delay changes in the vertical component. The measurement precision of the 3D baseline is 3.2, 3.8, and 26.0 mm. With the time delay variation compensation, it shows that the measurement result of the 3D baseline can keep stable. The measurement precision of the 3D baseline is 2.8, 3.6, and 2.0 mm.

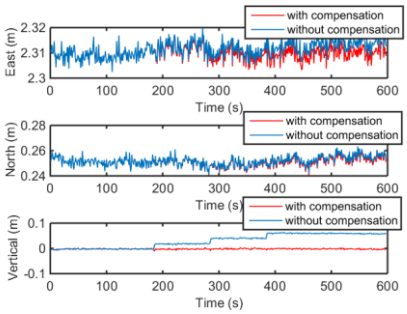


Fig. 7. Measurement results of the 3D displacement.

## IV. Conclusion

In conclusion, a 3D nodal displacement and distributed vibration sensing method was proposed for comprehensive structural health monitoring and risk prediction. With the high linearity LFM signal generated based on microwave photonic technology, vibrations with frequencies of 40 kHz, 80 kHz, and 100 kHz distributed along 250 m fiber are successfully detected, while the transmission delay between the antenna and receiver can also be measured with a precision of 3.03 ps. Based on the high-precision transmission delay, a GNSS-over-fiber based 3D displacement is simultaneously achieved with a precision of 2.8, 3.6, and 2.0 mm in three directions.

## References

[1] X. Wang et al., "An OTDR and gratings assisted multifunctional fiber sensing system," *IEEE Sensors J.*, vol. 15, no. 8, pp. 4660–4666, Aug. 2015.

[2] S. Yuezhen et al., "Excessively tilted fiber grating sensors," *J. Lightw. Technol.*, vol. 39, no. 12, pp. 3761–3770, Jun. 15, 2021.

[3] R. Ahmad, W. Ko, K. S. Feder, and P. S. Westbrook, "Measuring the shape of microbends in optical fibers," *Opt. Lett.*, vol. 45, no. 18, pp. 5189–5192, Sep. 2020.

[4] Y. Xu and J. M. W. Brownjohn, "Review of machine-vision based methodologies for displacement measurement in civil structures," *J. Civil Struct. Health Monitor.*, vol. 8, no. 1, pp. 91–110, 2018.

[5] D. V. Q. Rodrigues, D. Zuo, and C. Li, "Wind-induced displacement analysis for a traffic light structure based on a low-cost Doppler radar array," *IEEE Trans. Instrum. Meas.*, vol. 70, pp. 1–9, 2021.

[6] Z. Ma, J. Chung, P. Liu, and H. Sohn, "Bridge displacement estimation by fusing accelerometer and strain gauge measurements," *Struct. Control Health Monitor.*, vol. 28, no. 6, Jun. 2021.

[7] J. Yu, X. Meng, B. Yan, B. Xu, Q. Fan, and Y. Xie, "Global navigation satellite system-based positioning technology for structural health monitoring: A review," *Struct. Control Health Monit.*, vol. 27, no. 1, p. e2467, 2020.

[8] S. B. Im, S. Hurlebaus, and Y. J. Kang, "Summary review of GPS technology for structural health monitoring," *J. Struct. Eng.*, vol. 139, no. 10, pp. 1653–1664, 2013.

[9] P. Liu, Y. Li, X. Zou, J. Ye, W. Pan, and L. Yan, "Multi-antenna GNSS-over-fiber architecture for extensive remote multi-baseline network," *IEEE Photon. J.*, vol. 12, no. 3, pp. 1–10, Jun. 2020.

[10] X. Jiang, X. Wang, A. Zhao, J. Yao, and S. Pan, "A multi-antenna GNSS-over-fiber system for high accuracy three-dimensional baseline measurement," *J. Lightw. Technol.*, vol. 37, no. 17, pp. 4201–4209, Sep. 1, 2019.

[11] X. Wang et al., "High-accuracy optical time delay measurement in fiber link [Invited]," *Chin. Opt. Lett.*, vol. 17, no. 6, 2019, Art. no. 060601.

[12] Y. Zhang, C. Liu, K. Shao, Z. Li, and S. Pan, "Multioctave and reconfigurable frequency-stepped radar waveform generation based on an optical frequency shifting loop," *Opt. Lett.*, vol. 45, no. 7, pp. 2038–2041, 2020.

[13] Z. Ding et al., "Long-range vibration sensor based on correlation analysis of optical frequency-domain reflectometry signals," *Opt. Exp.*, vol. 20, no. 27, pp. 28319–28329, 2012.

Authorized licensed use limited to: NANJING UNIVERSITY OF AERONAUTICS AND ASTRONAUTICS. Downloaded on October 09,2024 at 02:38:19 UTC from IEEE Xplore. Restrictions apply.